Journal of Electromagnetic Waves and Applications, Vol. 13, 903–922, 1999

RADIATION AND RECEIVING CHARACTERISTICS OF PARALLEL PLATE-FED SLOT ANTENNAS LOADED BY A DIELECTRIC CYLINDER: TE-CASE

J. L. Tsalamengas and G. Veronis

Department of Electrical and Computer Engineering
National Technical University of Athens
9 Iroon Polytechniou Str., GR-15773
Athens, Greece

Abstract–In this paper, we present an exact analysis of parallel plate-fed slot antennas loaded by a dielectric cylinder. The primary excitation is taken to be either a TE incident mode of the parallel-plate waveguide or an incident E-polarized plane wave. The followed formulation technique leads to singular integral or integrodifferential equations of the first kind which are discretized using quasi-analytical methods. The matrix elements of the resulting system of linear algebraic equations are given either in closed form or via rapidly converging single series. This, in conjunction with the small matrix size required, enables one to obtain very accurate results with low computational cost. Typical numerical results are presented to bring to light the effect of the cylindrical load on the characteristics of the antenna.

1. INTRODUCTION

Waveguide radiators are extensively used in flush-mounted antennas and, also, in phased arrays. Usually, such antennas are dielectrically loaded either for impedance matching or for protection from the environment. In the majority of previous related papers, the load was taken to be either a dielectric half-space or infinitely extending dielectric slabs (see, e.g., [1–5] and references therein).

In this paper, we investigate the radiation and receiving characteristics of parallel plate-fed slot antennas loaded by an infinite dielectric cylinder, assuming (1) an incident TE-mode or (2) an incident E-polarized plane wave primary excitation.

A similar problem, dealing with this same structure loaded by a dielectric semi-cylinder which resides on the ground plane, has been treated in [6]. It should be noted, however, that the formulation technique followed in [6] was critically based on the availability of certain very suitable Green's functions. Lack of such Green's functions for the structure under consideration, renders that technique inapplicable here, necessitating recourse to other methods.

The analysis, carried out in section 2, leads to singular integral/integrodifferential equations of the fist kind. These equations are discretized with the help of quasi-analytical techniques, which yield efficient analytical expressions (either in closed form or in terms of rapidly converging single series) for all matrix elements. As a consequence of this and the small matrix sizes required, highly accurate results are obtainable with low computational cost. Typical numerical results are presented in section 3 which validate the algorithms and, also, show how—by suitably selecting the geometrical and physical parameters of the load- both the radiation and receiving efficiency of the antenna can be radically improved.

2. THE ANALYSIS

The geometry of the problem is shown in Fig. 1. The slot has width $2w$. The position of the cylinder of radius R is specified via the quantities (D, Φ). All three regions **a** $(z < 0)$, **0** $(\rho < R)$, and **1** $(z > 0, \rho > R)$, where ρ is measured from the axis of the cylinder as in Fig. 2, are taken to be linear, isotropic and homogeneous, characterized by the scalar constants $\left(\varepsilon_i, \mu_i, k_i = \omega\sqrt{\varepsilon_i\mu_i}\right)(i \equiv a, 0, 1)$.

The cases of **(1)** incident TE_{L0}-modes and **(2)** incident E-polarized plane waves will be treated on parallel lines in sections 2.A and 2.B below. In both cases, all fields involved in the analysis have the form $\overline{E} = \hat{y}E_y$, $\overline{H} = \hat{x}H_x + \hat{z}H_z$ where, assuming the $\exp(+j\omega t)$ time dependence,

$$\begin{aligned} H_x(x,z) &= \frac{1}{j\omega\mu_i}\frac{\partial E_y(x,z)}{\partial z}, \\ H_z(x,z) &= -\frac{1}{j\omega\mu_i}\frac{\partial E_y(x,z)}{\partial x}[(x,z) \in (i),\ i \equiv a, 0, 1]. \end{aligned} \tag{1}$$

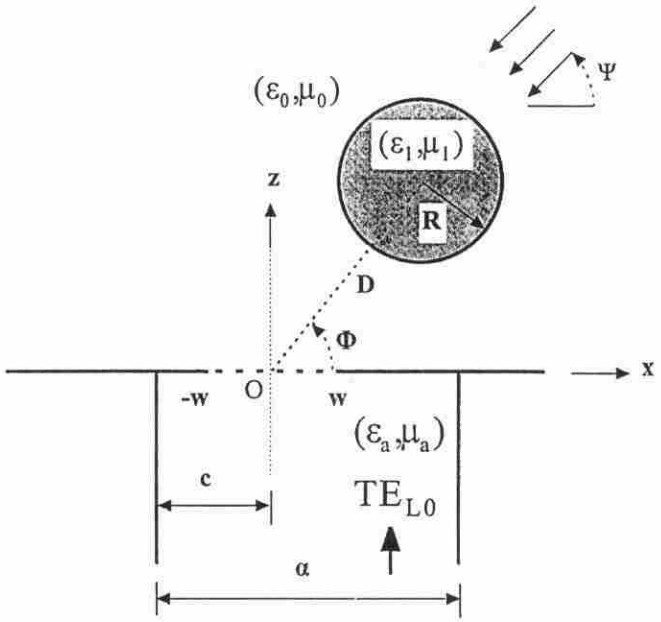

Figure 1. Geometry of the problem.

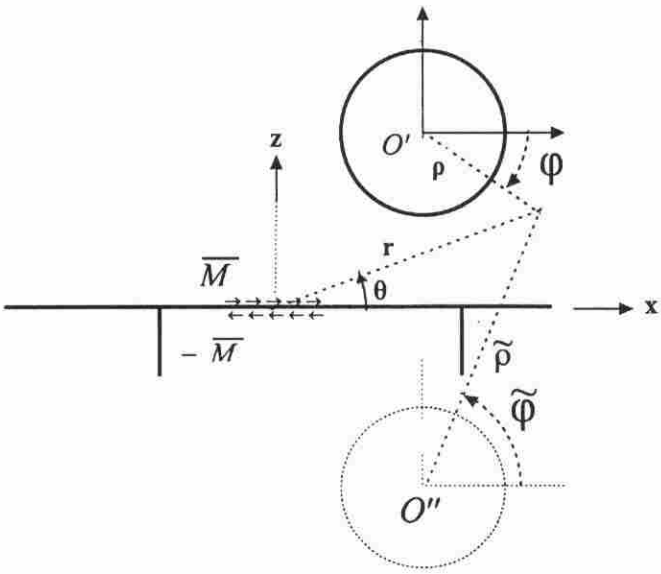

Figure 2. Equivalent problems for $z > 0$ and $z < 0$.

2.A Incident TE_{L0}-mode Primary Excitation

Let the TE_{L0}-mode be incident from below, then its electric field is given by

$$E_y^{inc}(x,z) = E_0\varphi_L(x)e^{-\gamma_L z/\alpha}, \qquad \varphi_L(x) = \sin\left(L\pi\frac{x+c}{\alpha}\right),$$
$$\gamma_L = \left[(L\pi)^2 - (k_a\alpha)^2\right]^{1/2}, \qquad 0 \le arg(\gamma_L) \le \pi/2 \tag{2}$$

The field $(\overline{E}^{exc} = \hat{y}E_y^{exc}, \overline{H}^{exc})$ excited by this incident mode when the slot is absent (short-circuited) will be termed excitation field. Its electric field is given by

$$E_y^{exc}(x,z) = -2E_0\varphi_L(x)\sinh(\gamma_L z/\alpha)(z \le 0),\ 0(z \ge 0). \tag{3}$$

The scattered field at points of region $\mathbf{i}(\mathbf{i} \equiv \mathbf{a}, \mathbf{0}, \mathbf{1})$ will be defined as the difference $(\overline{E}, \overline{H}) = \left(\overline{E}^{tot}, \overline{H}^{tot}\right) - \left(\overline{E}^{exc}, \overline{H}^{exc}\right)$ between the total and the excitation fields.

2.A.1 Representation of the Scattered Electric Field in Regions a, 0, 1

Taking advantage of the field equivalence principle, one may consider the equivalent problems shown in Fig. 2. The equivalent surface magnetic current densities $\pm\overline{M}(x)$, located at $z = 0\pm$, are defined by

$$\overline{M} = \overline{E}(x, z=0) \times \hat{z} = \hat{x}E_y(x, z=0) = \hat{x}M_x(x). \tag{4}$$

These magnetic currents are taken to radiate into regions $z > 0$ and $z < 0$, respectively, in the presence of a completely opaque ground plane (slot short-circuited).

The scattered electric field may then be expressed as follows.

Region a [6]

$$E_y^a(x,z) = -\int_{-w}^{w} M_x(x')\frac{\partial}{\partial z'}G\left(x', z'=0-; x, z\right)dx' \tag{5}$$

$$G(x,z;x',z') = \sum_{n=1}^{\infty}\frac{1}{\gamma_n}\varphi_n(x)\varphi_n(x')\left[e^{-\gamma_n|z-z'|/\alpha} - e^{-\gamma_n|z+z'|/\alpha}\right] \tag{6}$$

Region 1

$$E_y^1(x,z) = \sum_{n=-\infty}^{\infty} c_n J_n(k_1\rho)e^{jn\varphi} \tag{7}$$

where ρ, φ refer to the cylindrical coordinate system $O'(\rho, \varphi, y)$ centered at O'. In (7), c_n are expansion constants whereas J_n denotes the Bessel function of order n.

Region 0

$$E_y^0(x,z) = E_y^s(x,z) + E_y^c(x,z) \tag{8}$$

where [7]

$$E_y^s(x,z) = \frac{j}{2}\int_{-w}^{w} M_x(x')\frac{\partial}{\partial z}H_0^{(2)}\left(k_0\sqrt{(x-x')^2+z^2}\right)dx' \tag{9}$$

is due to the slot (surface magnetic current density M_x), whereas

$$E_y^c(x,z) = \sum_{n=-\infty}^{\infty} b_n\left[H_n^{(2)}(k_0\rho)e^{jn\varphi} - H_n^{(2)}(k_0\tilde{\rho})e^{-jn\tilde{\varphi}}\right] \tag{10}$$

is due to the presence of the dielectric cylinder (equivalent polarization current density). Here, $H_n^{(2)}$ is the second-kind Hankel function of order n, b_n are unknown expansion constants, whereas the cylindrical coordinates $O''(\tilde{\rho}, \tilde{\varphi}, y)$ are measured as in Fig. 2 (O'' is the image of O' with respect to the plane $z = 0$). The inclusion of the second Hankel term in the right side of (10) assures that E_y^c vanishes at $z = 0$, thus facilitating the application of the continuity condition for E_y at $z = 0$.

2.A.2 Integral Equations of the Problem

Via the representations (5), (7)–(10), it may be verified that the continuity of E_y at $z = 0$ is automatically satisfied. The remaining three boundary conditions of the problem: $H_x^a(x,0-) + H_x^{exc}(x,0-) = H_x^0(x,0+)(|x| \le w)$; $E_y^0(\rho = R, \varphi) = E_y^1(\rho = R, \varphi)$, $\hat{\varphi}\cdot\overline{H}^0(\rho = R, \varphi) = \hat{\varphi}\cdot\overline{H}^1(\rho = R, \varphi)(0 \le \varphi \le 2\pi)$ lead to three singular integral or integrodifferential equations of the first kind. Leaving aside all intermediate derivations, the final form of these equations is the following:

$$
\begin{aligned}
&-\frac{2j}{\omega\mu_a}\left(k_a^2+\frac{d^2}{dx^2}\right)\int_{-w}^{w} M_x(x')\sum_{n=1}^{\infty}\frac{1}{\gamma_n}\varphi_n(x)\varphi_n(x')dx' \\
&-\frac{1}{2\omega\mu_0}\left(k_0^2+\frac{d^2}{dx^2}\right)\int_{-w}^{w} M_x(x')H_0^{(2)}(k_0|x-x'|)dx' \\
&+\frac{1}{j\omega\mu_0}\sum_{n=-\infty}^{\infty} b_n\frac{\partial}{\partial z}\left[H_n^{(2)}(k_0\rho)e^{jn\varphi}-H_n^{(2)}(k_0\tilde{\rho})e^{-jn\tilde{\varphi}}\right]_{z=0} \\
&\quad = H_x^{exc}(x,0-) = -\frac{2E_0\gamma_L}{j\omega\mu_a\alpha}\varphi_L(x) \qquad (x|\le w), \qquad (11)
\end{aligned}
$$

$$
\begin{aligned}
&\sum_{n=-\infty}^{\infty} b_n\left[H_n^{(2)}(k_0\rho)e^{jn\varphi}-H_n^{(2)}(k_0\tilde{\rho})e^{-jn\tilde{\varphi}}\right]_{\rho=R} \\
&+\frac{j}{2}\int_{-w}^{w} M_x(x')\frac{\partial}{\partial z}H_0^{(2)}\left(k_0\sqrt{(x-x')^2+z^2}\right)\Big|_{\rho=R}dx' \\
&-\sum_{n=-\infty}^{\infty} c_nJ_n(k_1R)e^{jn\varphi}=0 \qquad (0\le\varphi\le 2\pi), \qquad (12)
\end{aligned}
$$

$$
\begin{aligned}
&\frac{1}{\mu_0}\frac{\partial}{\partial\rho}\left[\sum_{n=-\infty}^{\infty} b_n\left[H_n^{(2)}(k_0\rho)e^{jn\varphi}-H_n^{(2)}(k_0\tilde{\rho})e^{-jn\tilde{\varphi}}\right]\right. \\
&\left.+\frac{j}{2}\int_{-w}^{w} M_x(x')\frac{\partial}{\partial z}H_0^{(2)}\left(k_0\sqrt{(x-x')^2+z^2}\right)dx'\right]_{\rho=R} \\
&-\frac{k_1}{\mu_1}\sum_{n=-\infty}^{\infty} c_nJ_n'(k_1R)e^{jn\varphi}=0 \qquad (0\le\varphi\le 2\pi) \qquad (13)
\end{aligned}
$$

2.A.3 Discretization of Equations (11), (12), (13)

The unknown surface magnetic current density will be sought in the form

$$
M_x(x') = M_x[x(t')] = \sqrt{1-t'^2}\sum_{N=0}^{\infty} a_NU_N(t')(t'\equiv x'/w) \qquad (14)
$$

satisfying via the weighting factor $(1-t'^2)^{1/2}$ the edge condition. In (14), U_N is the Chebyshev polynomial of the second kind.

The unknown expansion constants $\{a_N, b_n, c_n\}$ will be found after discretization of the system of equations (11), (12), and (13) as described below.

Equation (11)

We set $x = wt$, $x' = wt'(-1 \leq t, t' \leq 1)$. Substituting from (14) into (11), multiplying both sides by $\sqrt{1-t^2}U_M(t)$ and integrating from $t=-1$ to $t=1$, one ends up with the linear algebraic equations

$$\sum_{N=0}^{\infty} a_N \tilde{A}^{11}_{MN} + \sum_{n=-\infty}^{\infty} b_n \tilde{A}^{12}_{Mn} = \tilde{D}^1_M, \qquad M = 0, 1, 2, \ldots \tag{15}$$

where

$$\tilde{D}^1_M = E_0 j^M \frac{\gamma_L}{Lw\omega\mu_\alpha}(M+1)c_{M+1}(L) \tag{16}$$

$$c_M(L) = \left[e^{jL\pi c/\alpha} + (-1)^M e^{-jL\pi c/\alpha}\right] J_M(L\pi w/\alpha). \tag{17}$$

The matrix elements $\tilde{A}^{11}_{MN}$ are given by

$$\tilde{A}^{11}_{MN} = \frac{1}{\omega}\tilde{K}^a_{MN} - \frac{1}{2\omega\mu_0 w}\tilde{K}_{MN}(k_0 w) \tag{18}$$

where $\tilde{K}^a_{MN}$ and $\tilde{K}_{MN}(k_0 w)$ are given in Appendix A.

Evaluation of $\tilde{A}^{12}_{Mn}$

The evaluation of

$$\begin{aligned}\tilde{A}^{12}_{Mn} &\equiv \frac{1}{j\omega\mu_0}\int_{-1}^{1} dt\sqrt{1-t^2}U_M(t)\frac{\partial}{\partial z} \\ &\quad \cdot \left[H^{(2)}_n(k_0\rho)e^{jn\varphi} - H^{(2)}_n(k_0\tilde{\rho})e^{-jn\tilde{\varphi}}\right]_{z=0} \\ &= \frac{2}{j\omega\mu_0}\int_{-1}^{1} dt\sqrt{1-t^2}U_M(t)\frac{\partial}{\partial z}\left[H^{(2)}_n(k_0\rho)e^{jn\varphi}\right]_{z=0}\end{aligned} \tag{19}$$

is carried out as follows.

a. $w < D$ case : In this case the expansion

$$H_n^{(2)}(k_0\rho)e^{jn\varphi} = \sum_{m=-\infty}^{\infty} H_{n-m}^{(2)}(k_0 D)J_m(k_0 r)e^{jm\theta}e^{j(n-m)(\pi+\Phi)} \tag{20}$$

is valid, leading—via (19) with the help of the relation $\frac{\partial}{\partial z}\big|_{z=0} = \frac{1}{x}\frac{\partial}{\partial \theta}$ — to the result

$$\tilde{A}_{Mn}^{12} = \frac{1}{Z_0}\sum_{m=-\infty}^{\infty} H_{n-m}^{(2)}(k_0 D)J^+(M,m)e^{j(n-m)(\pi+\Phi)} \tag{21a}$$

$$= \frac{1}{Z_0}\sum_{m=1}^{\infty}\Big[H_{n-m}^{(2)}(k_0 D)e^{j(n-m)(\pi+\Phi)} - (-1)^m \cdot H_{n+m}^{(2)}(k_0 D)e^{j(n+m)(\pi+\Phi)}\Big] J^+(M,m). \tag{21b}$$

Here,

$$Z_0 = \sqrt{\frac{\mu_0}{\varepsilon_0}}, \qquad J^+(M,m) = J(M,m-1) + J(M,m+1) \tag{22}$$

$$J(p,q) \equiv \int_{-1}^{1}\sqrt{1-t^2}U_p(t)J_q(k_0 w t)dt = \frac{1}{2}\left[I(p,q) - I(p+2,q)\right] \tag{23}$$

$$I(p,q) \equiv \int_{-1}^{1}\frac{1}{\sqrt{1-t^2}}T_p(t)J_q(k_0 w t)dt = \pi\begin{cases} J_{\frac{p+q}{2}}(k_0 w/2)J_{\frac{q-p}{2}}(k_0 w/2), & p+q \text{ even} \\ 0, & p+q \text{ odd} \end{cases} \tag{24}$$

where in (24) T_p is the Chebyshev polynomial of the first kind.

b. general case : An alternative method to evaluate $\tilde{A}_{Mn}^{12}$, free of any limitations (i.e., valid for $w \geq D$ as well as for $w < D$), is based on Lobatto's integration formula [8]

$$\int_{-1}^{1}\sqrt{1-t^2}f(t)dt = \frac{\pi}{m+1}\sum_{i=1}^{m}\sin^2(\theta_i)f(t_i), \quad t_i = \cos\theta_i, \quad \theta_i \equiv \frac{i\pi}{m+1}, \tag{25}$$

where m is a fixed integer selected as high as needed to assure any prescribed accuracy. Using (25) we end up with the result

$$\tilde{A}^{12}_{Mn} = \frac{2\pi}{m+1}\frac{1}{j\omega\mu_0}\sum_{i=1}^{m}\sin^2(\theta_i)F(t_i) \tag{26}$$

where

$$F(t_i) = U_M(t_i)\frac{e^{jn\varphi_i}}{\rho_i}\left[-k_0 D\sin\Phi H_n'^{(2)}(k_0\rho_i) + \frac{jn}{\rho_i}(wt_i - D\cos\Phi)H_n^{(2)}(k_0\rho_i)\right] \tag{27}$$

with

$$\begin{aligned}\rho_i &= \sqrt{(wt_i)^2 - 2wt_i D\cos\Phi + D^2},\\ \varphi_i &= \tan^{-1}(-D\sin\Phi, wt_i - D\cos\Phi),\\ U_M(t_i) &= \sin[(M+1)\theta_i]/\sin\theta_i.\end{aligned} \tag{28}$$

In (28), the function $\tan^{-1}(y,x)$ is implemented by the DATAN2 (y,x) routine of FORTRAN.

Equation (12)

Substituting from (14) into (12), multiplying both sides by $e^{-jM\varphi}/(2\pi)$ and integrating from $\varphi = 0$ to $\varphi = 2\pi$, we end up with the linear algebraic equations

$$\sum_{N=0}^{\infty} a_N \tilde{A}^{21}_{MN} + \sum_{n=-\infty}^{\infty} b_n \tilde{A}^{22}_{Mn} + \sum_{n=-\infty}^{\infty} c_n \tilde{A}^{23}_{Mn} = \tilde{D}^2_M,\ M = 0, \pm 1, \pm 2, \ldots \tag{29}$$

where

$$\tilde{D}^2_M = 0 \tag{30}$$

$$\tilde{A}^{23}_{Mn} = -J_M(k_1 R)\delta_{nM} \tag{31}$$

δ_{nM} being the Kronecker delta. The evaluation of $\tilde{A}^{22}_{Mn}$ is facilitated by the use of the expansion

$$H_n^{(2)}(k_0\tilde{\rho})e^{-jn\tilde{\varphi}}\Big|_{\rho=R} = \sum_{m=-\infty}^{\infty} H^{(2)}_{n-m}(2k_0 D\sin\Phi)J_m(k_0 R)e^{-jm\varphi}j^{m-n} \tag{32}$$

which, based on the addition theorem for Hankel functions [8], is valid for any combinations of the geometrical parameters of the structure. The final result is the following closed form expression

$$\tilde{A}^{22}_{Mn} = -(-1)^n H^{(2)}_{n+M}(2k_0 D\sin\Phi) J_M(k_0 R) j^{n+M} + H^{(2)}_M(k_0 R)\delta_{nM}. \tag{33}$$

Evaluation of $\tilde{A}^{21}_{MN}$

a. **w < D case**: In this case, with the help of Appendix B equations (61)–(64), we get the result

$$\tilde{A}^{21}_{MN} = J_M(k_0 R)\tilde{F}_{MN} \tag{34}$$

where

$$\tilde{F}_{MN} = \frac{wk_0}{4}(-1)^M \sum_{\ell=-\infty}^{\infty} J^+(N,\ell) e^{-j(M+\ell)\Phi} H^{(2)}_{M+\ell}(k_0 D). \tag{35}$$

b. **general case**: An alternative method to evaluate $\tilde{A}^{12}_{MN}$, free of any limitations (i.e., valid for $w \geq D - R$ as well as for $w < D - R$) is based on Appendix B equation (61)–(62) in conjunction with Lobatto's integration formula (25). The final result is the expression

$$\tilde{A}^{21}_{MN} = J_M(k_0 R)\tilde{G}_{MN} \tag{36}$$

where

$$\tilde{G}_{MN} = \frac{jw}{2}\frac{\pi}{m+1}\sum_{i=1}^{m} \sin^2(\theta_i) U_N(t_i) \frac{e^{-jM\varphi_i}}{\rho_i} \cdot \left[k_0 D\sin\Phi H^{\prime(2)}_M(k_0\rho_i) + \frac{jM}{\rho_i}(wt_i - D\cos\Phi) H^{(2)}_M(k_0\rho_i)\right] \tag{37}$$

with ρ_i and φ_i defined in (28).

Equation(13)

This equation can be treated in analogy with (12), leading to the following linear algebraic equations

$$\sum_{N=0}^{\infty} a_N \tilde{A}^{31}_{MN} + \sum_{n=-\infty}^{\infty} b_n \tilde{A}^{32}_{Mn} + \sum_{n=-\infty}^{\infty} c_n \tilde{A}^{33}_{Mn} = \tilde{D}^3_M, \quad M = 0, \pm 1, \pm 2, \ldots \tag{38}$$

where

$$\tilde{D}_M^3 = 0 \tag{39}$$

$$\tilde{A}_{Mn}^{33} = -\frac{k_1}{\mu_1} J'_M(k_1 R)\delta_{nM} \tag{40}$$

$$\tilde{A}_{Mn}^{32} = \frac{k_0}{\mu_0}\left[-(-1)^n H_{n+M}^{(2)}(2k_0 D\sin\Phi) J'_M(k_0 R) j^{n+M} + H_M^{\prime(2)}(k_0 R)\delta_{nM}\right]. \tag{41}$$

Finally, $\tilde{A}_{MN}^{31}$ takes either the expression

$$\tilde{A}_{MN}^{31} = \frac{k_0}{\mu_0} J'_M(k_0 R)\tilde{F}_{MN}, \tag{42}$$

with $\tilde{F}_{MN}$ defined in (35), or the expression

$$\tilde{A}_{MN}^{31} = \frac{k_0}{\mu_0} J'_M(k_0 R)\tilde{G}_{MN} \tag{43}$$

with $\tilde{G}_{MN}$ defined in (37). Equation (43) is subject on the restriction $w < D - R$ whereas (42) has no limitation.

The unknown expansion coefficients are determined from the system of equations (15), (29), and (38). In terms of them any quantity of practical interest can be found as described in section 3.

2.B *E*-Polarized Plane Wave Excitation

We consider now the following E-polarized plane-wave

$$\begin{aligned} \overline{E}^{inc} &= \hat{y} E_0 e^{-jk_0 \hat{k}^{inc}\cdot\overline{r}}, \\ \overline{H}^{inc} &= \left(\hat{k}^{inc} \times \overline{E}^{inc}\right)/Z_0, \\ \hat{k}^{inc} &= -\hat{x}\cos\psi - \hat{z}\sin\psi \end{aligned} \tag{44}$$

incident from region **0** in the direction of $\hat{k}^{inc}$. In this case we will define the "excitation field" as the field excited by the incident plane wave, in the absence of the cylinder, when the slot is short-circuited. Its electric field is given by

$$E_y^{exc}(x,z) = 2jE_0 e^{jk_0 x\cos\psi}\sin(k_0 z\sin\psi) \quad (z>0),\ 0(z<0). \tag{45}$$

The scattered field at points of regions **a, 0, 1** is again expressible via (4), (7), (8).

The boundary conditions of the problem, $H_x^{(a)}(x,0-) = H_x^{(0)}(x,0+) + H_x^{exc}(x,0+)(|x| \le w)$; $E_y^{(0)} + E_y^{exc} = E_y^{(1)}$, $\hat{\varphi}\cdot\overline{H}^{(0)} + \hat{\varphi}\cdot\overline{H}^{exc} = \hat{\varphi}\cdot\overline{H}^{(1)}(\rho = R, 0 \le \varphi \le 2\pi)$ lead to three integral/integrodifferential equations which are identical with those of (11), (12), (13) with the following exceptions: **(a)** the right side term $H_x^{exc}(x,0-)$ of (11) is now replaced by $-H_x^{exc}(x,0+)$ (evaluated from (1) with the help of (45)), **(b)** the right side of (12) is $-E_y^{exc}(R,\varphi)$ instead of 0, **(c)** the right side of (13) is $-\frac{1}{\mu_0}\hat{\varphi}\cdot\overline{H}^{exc}(R,\varphi)$.

Discretization of the above equations as outlined in the preceding subsection 2.A yields again the system of linear algebraic equations (15), (29), (38). All matrix elements retain their expressions derived in section 2.A whereas the constant terms $\tilde{D}_M^1$, $\tilde{D}_M^2$, $\tilde{D}_M^3$ are now given by

$$\tilde{D}_M^1 = -E_0\frac{2}{Z_0}\frac{\sin\psi}{k_0 w\cos\psi}\pi j^M(M+1)J_{M+1}(k_0 w\cos\psi), \qquad M = 0,1,2,\ldots \tag{46}$$

$$\tilde{D}_M^2 = -E_0 j^M J_M(k_0 R)G_M, \qquad M = 0,\pm1,\pm2,\ldots \tag{47}$$

$$\tilde{D}_M^3 = -\frac{k_0}{\mu_0}E_0 j^M J_M'(k_0 R)G_M, \qquad M = 0,\pm1,\pm2,\ldots \tag{48}$$

with

$$G_M \equiv e^{jk_0 D\cos(\Phi-\psi)}e^{-jM\psi} - e^{jk_0 D\cos(\Phi+\psi)}e^{jM\psi} \tag{49}$$

2.C Scattered Fields

The scattered electric field at any point in region **a** is given by

$$E_y^{(a)}(x,z) = \sum_{n=1}^{\infty} T_{0n}^{TE}\varphi_n(x)e^{\gamma_n z/\alpha} \tag{50}$$

where

$$T_{0n}^{TE} = \frac{1}{n}\sum_{N=0}^{\infty} a_N j^{N-1}(N+1)c_{N+1}(n) \tag{51}$$

with c_N defined in (17). In the case of the incident TE_{L0} mode (section 2.A) the reflection coefficient of this mode is given by

$$R_{L0}^{TE} = -1 + T_{0L}^{TE}. \tag{52}$$

The far scattered electric field in region **0** in polar coordinates $O(r,\theta)$ and the per unit length far radiated power are given by the relations

$$E_y^{(0)}(r,\theta) = \sqrt{\frac{2}{\pi k_0 r}} e^{-j\left(k_0 r - \frac{\pi}{4}\right)} \cdot \left(-\frac{1}{4} k_0 w \sum_{N=0}^{\infty} a_N \left[J^+(N,0) + 2j \sum_{m=1}^{\infty} J^+(N,m) j^m \sin(m\theta) \right] + 2j \sum_{n=-\infty}^{\infty} b_n \sum_{m=-\infty}^{\infty} J_m(k_0 D) e^{jm(\pi+\Phi)} \sin[(n-m)\theta] j^{n-m} \right) \quad (53)$$

$$P_{rad} = \frac{1}{2Z_0} \int_o^{\pi} r \left| E_y^{(0)}(r,\theta) \right|^2 d\theta \quad (54)$$

3. NUMERICAL RESULTS AND DISCUSSION

Sample numerical results are presented below for the parameter values $\mu_\alpha = \mu_1 = \mu_0$, $c/\alpha = 0.5$, $w/\alpha = 0.25$, $E_0 = 1\,\mathrm{V/m}$, assuming that region **0** is air.

3.A Convergence of the Matrix Elements

Table 1 presents values of the matrix element $\tilde{A}_{00}^{12}$ as obtained (a) via (21b), using $m_{\max}$ series terms, and (b) from (26) for several values of m. The parameter values are $D = 0.4\lambda$, $w = 0.2\lambda$, $\Phi = \pi/2$ (λ is the free-space wavelength). From this table we observe, e.g., that using $m_{\max} = 40$ series terms in (21b) or $m = 12$ in (26) assures an accuracy to within 16 significant decimals. The convergence of other matrix elements was found to be similar (not shown).

3.B Convergence and Validation of the Algorithm

The convergence of the algorithm will be illustrated in connection with the following truncated form of the linear algebraic system of equations (15), (29), and (38):

$$\sum_{N=0}^{N_1-1} a_N \tilde{A}_{MN}^{11} + \sum_{n=-N_2}^{N_2} b_n \tilde{A}_{Mn}^{12} = \tilde{D}_M^1, \quad M = 0,1,2,\ldots,N_1-1 \quad (55a)$$

$m_{\max}$	$\tilde{A}_{00}^{12}$ of equation (21b)
10	$-0.00147666424863165 - j0.00383538534264153$
20	$-0.00147674549731481 - j0.00383538534264153$
25	$-0.00147674546876499 - j0.00383538534264153$
30	$-0.00147674546904863 - j0.00383538534264153$
35	$-0.00147674546906390 - j0.00383538534264153$
40	$-0.00147674546906373 - j0.00383538534264153$
45	$-0.00147674546906373 - j0.00383538534264153$
m	$\tilde{A}_{00}^{12}$ of equation (26)
4	$-0.00147677815047212 - j0.00383538508578739$
6	$-0.00147674555414627 - j0.00383538534263939$
8	$-0.00147674546930824 - j0.00383538534264153$
10	$-0.00147674546906445 - j0.00383538534264153$
12	$-0.00147674546906373 - j0.00383538534264153$
14	$-0.00147674546906373 - j0.00383538534264153$

Table 1. Convergence of $\tilde{A}_{00}^{12}$ for $D = 0.4\lambda$, $\Phi = \pi/2$, $w = 0.2\lambda$.

$$\sum_{N=0}^{N_1-1} a_N \tilde{A}_{MN}^{21} + \sum_{n=-N_2}^{N_2} b_n \tilde{A}_{Mn}^{22} + \sum_{n=-N_2}^{N_2} c_n \tilde{A}_{Mn}^{23} = \tilde{D}_M^2, \quad M = 0, \pm 1, \pm 2, \ldots, \pm N_2 \tag{55b}$$

$$\sum_{N=0}^{N_1-1} a_N \tilde{A}_{MN}^{31} + \sum_{n=-N_2}^{N_2} b_n \tilde{A}_{Mn}^{32} + \sum_{n=-N_2}^{N_2} c_n \tilde{A}_{Mn}^{33} = \tilde{D}_M^3, \quad M = 0, \pm 1, \pm 2, \ldots, \pm N_2 \tag{55c}$$

The convergence versus truncation sizes N_1 and N_2 is illustrated in Table 2 where the radiation efficiency P_{rad}/P_{inc} is shown for the TE_{10} incident mode when $\alpha = 0.8\lambda$, $D = \lambda$, $R = 0.3\lambda$, $\Phi = \pi/2$, $\varepsilon_a = \varepsilon_0$, $\varepsilon_r = \varepsilon_1/\varepsilon_0 = 2$. As seen, the convergence is stable and rapid (for instance, using $N_1 = N_2 = 10$ assures an accuracy to within 13 significant figures).

In the case of a TE incident mode, a validity test that has been extensively used was based on energy conservation principle: $P_{inc} = P_{refl} + P_{rad}$. In the case of an incident plane wave primary excitation, the algorithm was tested by verifying the validity of the relation

$N_1 = N_2$	P_{rad}/P_{inc}
5	0.5245025390926
10	0.5245025263801
20	0.5245025263801

Table 2. Convergence of P_{rad}/P_{inc} for the TE_{10} incident mode at $\alpha = 0.8\lambda$, $D = \lambda$, $R = 0.3\lambda$, $\Phi = \pi/2$, $\varepsilon_r = 2$.

$E_y^{(0)}(r, \theta = \theta_0; \psi = \psi_0) = E_y^{(0)}(r, \theta = \psi_0; \psi = \theta_0)$, based on the reciprocity theorem. In all numerous cases that have been considered both these relations were ascertained to within at least 13 significant decimals.

3.C Further Numerical Results

For the TE_{10} incident mode, Fig. 3 shows the radiation efficiency (P_{rad}/P_{inc}) versus D/λ, R/λ, ε_r, and α/λ when $\varepsilon_a/\varepsilon_0 = 3.7$ (the other parameter values are indicated in the insets). For the sake of comparisons, the case $\varepsilon_r = 1 \backslash R = 0$ (unloaded antenna) is also included. We observe that, for the parameter values selected, the unloaded antenna is a poor radiator over the entire frequency range. In contrast, by properly selecting the geometrical and physical parameters of the load a very high efficiency is attainable. For instance, the choice $\alpha/\lambda = 0.6349$, $R/\lambda = 0.301$, $D/\lambda = 0.371$, $\varepsilon_r = 6.84$ leads to an almost perfect matching ($P_{rad}/P_{inc} > 99.89\%$).

Fig. 4 shows the radiation efficiency versus $\varepsilon_{ra} \equiv \varepsilon_a/\varepsilon_0$ for $\alpha = 0.56\lambda$, $R = 0.301\lambda$, $D = 0.371\lambda$, $\Phi = \pi/2$, $\varepsilon_r = 6.84$ (solid line). For comparison, the case $\varepsilon_r = 1 \backslash R = 0$ (unloaded antenna) is also included (dotted line). Clearly, for this selection of the parameter values, the presence of the dielectric cylinder greatly improves the efficiency of the antenna for any choice of ε_a.

The receiving characteristics of the structure are illustrated in Fig. 5 where the per unit length normalized receiving cross section (σ_R/w) is shown as a function of ε_r in case of an incident plane wave for $f = 10\,\mathrm{GHz}$, $\Phi = \pi/2$, $\Psi = \pi/4$, $\alpha = 0.56\lambda$, $R = 0.301\lambda$, $D = 0.371\lambda$, $\varepsilon_a = \varepsilon_0$. The receiving cross section is defined by

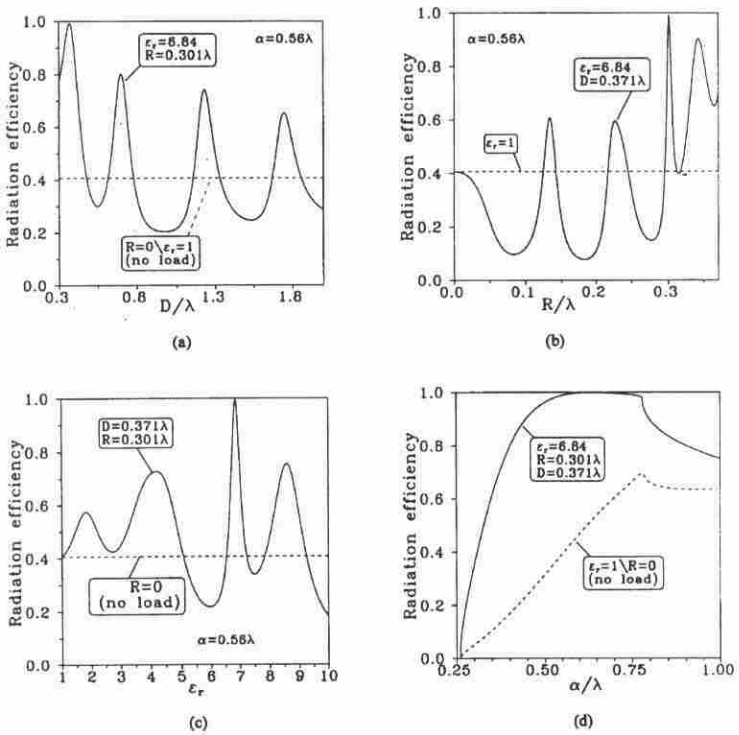

Figure 3. Radiation efficiency (P_{rad}/P_{inc}) versus D/λ, R/λ, ε_r, and α/λ.

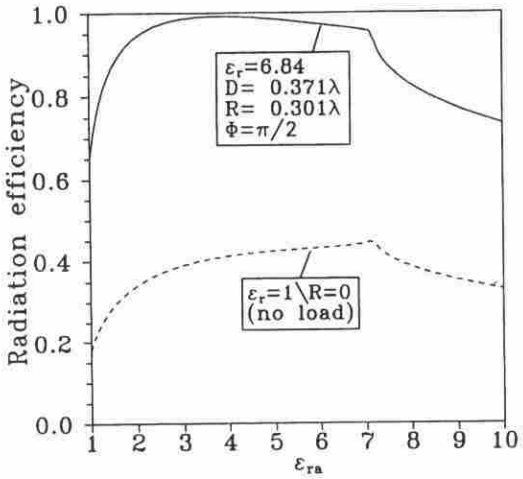

Figure 4. Radiation efficiency versus ε_{ra} (solid curve: loaded antenna, dotted curve: unloaded antenna).

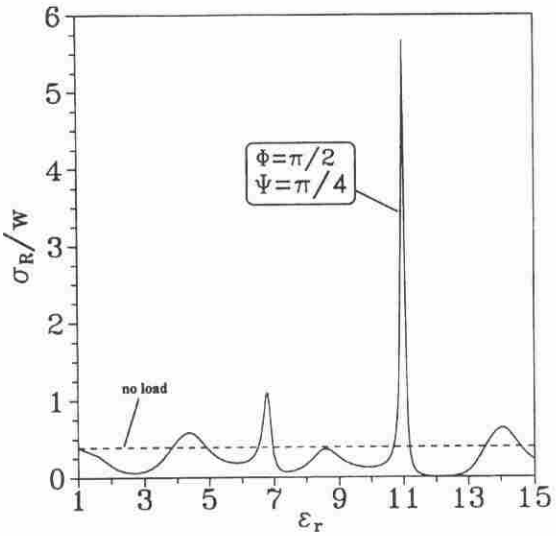

Figure 5. Normalized receiving cross section σ_R/w versus ε_r .

$$\sigma_R = \frac{\textit{Power} \text{ received by the antenna}}{\textit{incident} \text{ power density}} = \frac{P_{rec}}{\dfrac{1}{2Z_0}|E_0|^2} \tag{56}$$

where

$$P_{rec} = \sum_{n=0}^{N_{prop}} |T_{0n}^{TE}|^2 \frac{|\gamma_n|}{4\omega\mu_\alpha} \tag{57}$$

with T_{0n}^{TE} given by (51) and with N_{prop} denoting the number of propagating waveguide modes. From this figure, we conclude that by properly selecting the values of the geometrical parameters of the load the receiving efficiency may be radically improved. For instance, whereas $\sigma_R/w = 0.3909$ for $\varepsilon_r = 1$ (unloaded antenna), the presence of a dielectric cylinder of relative dielectric permittivity $\varepsilon_r = 11$ leads to the value $\sigma_R/w = 5.669$ (i.e., the receiving efficiency has been improved by the factor 14.5).

4. CONCLUSION

Rapidly converging semi-analytical methods have been used to analyze the parallel plate-fed slot antenna loaded by a dielectric cylinder assuming either a TE incident mode or an E-polarized plane wave primary excitation. These techniques yield either closed form or rapidly converging series expressions for all matrix elements. Proper choice of the geometrical and physical parameters of the load results in a radical improvement in both the radiation and receiving efficiency of the antenna.

APPENDIX A

Expression of $\tilde{K}^a_{MN}$

$$\tilde{K}^a_{MN} = -\frac{1}{w\mu_\alpha} j^{M+N+1}(M+1)(N+1)\tilde{S}^a_{M+1,N+1} \tag{58}$$

$$\tilde{S}^a_{MN} = \sum_{n=1}^{\infty} \frac{\gamma_n}{n^2} J_M\left(\frac{n\pi w}{\alpha}\right) J_N\left(\frac{n\pi w}{\alpha}\right) \cdot \begin{cases} (-1)^M + \cos(2n\pi c/\alpha), & M+N \text{ even} \\ j\sin(2n\pi c/\alpha), & M+N \text{ odd} \end{cases} \tag{59}$$

Series $\tilde{S}^a_{MN}$, which converges very slowly (as n^{-2}), may be recast into rapidly converging series as described in [6, section III]. It is important to note that, using its accelerated form, $\tilde{S}^a_{MN}$ requires no more than 10–20 series terms in order to obtain results accurate within 15 significant decimals.

Expression of $\tilde{K}_{MN}(k_0 w)$

$$\tilde{K}_{MN}(k_0 w) \equiv \int_{-1}^{1} dt \sqrt{1-t^2} U_M(t) \left[\frac{d^2}{dt^2} + (k_0 w)^2\right] \int_{-1}^{1} dt' \sqrt{1-t'^2} U_N(t') H_0^{(2)}(k_0 w|t-t'|) \tag{60}$$

has been evaluated in [9]. It is identified with $\tilde{K}^s_{MN} + \tilde{K}^r_{MN}$ of [9], whose expressions [9, (25)–(26)] are exponentially converging, stable and numerically very efficient as discussed in detail in [9].

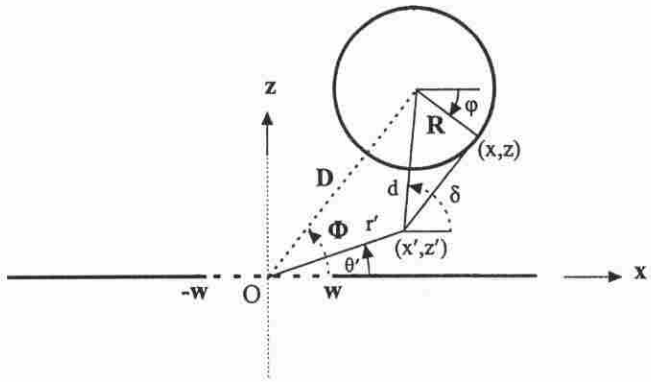

Figure 6. Specification of the geometrical parameters encountered in Appendix B equations.

APPENDIX B

With reference to Fig. 6 the following relations are valid:

$$\frac{\partial}{\partial z}H_0^{(2)}\left[k_0\sqrt{(x-x')^2+z^2}\right]_{\rho=R} = -\frac{\partial}{\partial z'}H_0^{(2)}\left[k_0\sqrt{(x-x')^2+(z-z')^2}\right]_{\rho=R,z'=0} \tag{61}$$

$$H_0^{(2)}\left[k_0\sqrt{(x-x')^2+(z-z')^2}\right]_{\rho=R} = \sum_{m=-\infty}^{\infty} H_m^{(2)}(k_0d)J_m(k_0R)e^{jm\varphi}e^{jm(\pi-\delta)} \qquad (d>R) \tag{62}$$

$$H_m^{(2)}(k_0d)e^{-jm\delta} = \sum_{\ell=-\infty}^{\infty} H_{m+\ell}^{(2)}(k_0D)J_\ell(k_0r')e^{j\ell\theta'}e^{-j(m+\ell)\Phi} \qquad (D>r') \tag{63}$$

$$\left.\frac{\partial}{\partial z'}\right|_{z'=0} = \frac{1}{x'}\frac{\partial}{\partial\theta'} \tag{64}$$

REFERENCES

1. Wu, C. P., "Integral equation solutions for the radiation from a waveguide through a dielectric slab," *IEEE Trans. Antennas Propagat.*, Vol. 17, 733–739, Nov. 1969.

2. Wu, C. P., "Numerical solutions for the coupling between waveguides in finite arrays," *Radio Sci.,* Vol. 4, No. 3, 245–254, Mar. 1969.
3. Hongo, K., "Diffraction by a flanged parallel-plate waveguide," *Radio Sci.,* Vol. 7, 955–963, Oct. 1972.
4. Park, T. J., and H. J. Eom, "Analytic solution for TE-mode radiation from a flanged parallel-plate waveguide," *IEE Proc., pt. H,* Vol. 140, No. 5, 387–389, Oct. 1993.
5. Scharstein, R. W., "Two numerical solutions for the parallel plate-fed slot antenna," *IEEE Trans. Antennas Propagat.,* Vol. 37, 1415–1426, Nov. 1989.
6. Tsalamengas, J. L., "A parallel plate-Fed slot antenna loaded by a dielectric semicylinder," *IEEE Trans. Antennas Propagat.,* Vol. 44, No. 7, 1031–1040, July 1996.
7. Tsalamengas, J. L., "TE/TM electromagnetic scattering by a slot on a ground plane and in the presence of a semi-cylindrical load," *JEWA,* Vol. 8, No. 5, 613–646, 1994.
8. Abramowitz, M., and I. A. Stegun, *Handbook of Mathematical Functions,* New York: Dover, 1972.
9. Tsalamengas, J. L., and J. G. Fikioris, "Efficient solutions for scattering from strips and slots in the presence of a dielectric half-space: Extension to wide scatterers -Part I: Theory," *J. Appl. Phys.,* Vol. 70, No. 3, 1121–1131, Aug. 1991.

J. L. Tsalamengas was born in Karditsa, Greece, in 1953. He received the Diploma of Electrical and Mechanical Engineering and the doctor's degree in Electrical Engineering from the National Technical University of Athens (NTUA), Greece, in 1977 and 1983, respectively. Since November 1995 he has been a Professor of Electrical Engineering at the NTUA where he has been teaching since 1984. His fields of interest include problems of wave propagation, radiation and scattering in the presence of complex media, computation electromagnetic, and applied mathematics.

Georgios Veronis was born on January 11, 1975 in Athens, Greece. He received the B.S. degree in Electrical Engineering from the National Technical University of Athens in 1997. He is currently working toward the M.S. degree in Electrical Engineering at Stanford University. His research interests include computational electromagnetics, plasma physics and applications.